JSTARS-2024-02655

An automatic decision-level fusion rice mapping method of optical and SAR images based on cloud coverage

Xueqin Jiang, Song Gao, Huaqiang Du, Shenghui Fang, Yan Gong, Ning Han, and Yirong Wang

***Abstract*—Timely and accurate mapping of paddy rice cultivation is crucial for estimating rice production and optimizing land utilization. Optical images are essential data source for paddy rice mapping, but it is susceptible to cloud contamination. Existing methods struggle to effectively utilize clear-sky pixel information in optical images containing clouds, which impacts the accuracy of paddy rice mapping under cloudy conditions. To address the above problems, we propose an automatic decision-level fusion rice mapping method of optical and synthetic aperture radar (SAR) images based on cloud coverage (the Auto-OSDF method). The method effectively utilizes clear-sky pixels in images containing clouds and leverages the advantages of SAR features in heavily clouded regions. We tested and validated the Auto-OSDF method in Xiangyin County, Hunan Province, and analyzed the impact of different cloud coverage levels (10% to 50%) on the accuracy of rice mapping based on this method. The results indicate that, as cloud coverage increases, the rice mapping accuracy of the Auto-OSDF method is not significantly affected, with overall accuracy and Kappa coefficients both above 93% and 0.90, respectively. To show the value of the proposed method in large-scale applications, we further mapped paddy rice in the entire Hunan Province, and the overall accuracy and Kappa coefficient were 92.47% and 0.87, respectively. The results obtained by the Auto-OSDF method show an average R^2 of 0.926 compared to municipal-level statistical planting areas. The above study demonstrates that the Auto-OSDF method is capable of achieving stable and high-precision rice mapping under cloud contamination interference.**

***Index Terms*—Paddy rice mapping; Cloud coverage; Optical and SAR images; Decision-level fusion; Time series**

Manuscript received 15 June 2024;******. This work was supported in part by the Research Development Fund of Zhejiang A & F University (2023LFR031) and in part by Scientific Research Fund of Zhejiang Provincial Education Department (Y202351543). *(Corresponding author: Song Gao).*

Xueqin Jiang, Huaqiang Du, Ning Han, and Yirong Wang are with the State Key Laboratory of Subtropical Silviculture, Zhejiang A & F University, Hangzhou 311300, China; the Key Laboratory of Carbon Cycling in Forest Ecosystems and Carbon Sequestration of Zhejiang Province, Zhejiang A & F University, Hangzhou 311300, China; and also with the School of Environmental and Resources Science, Zhejiang A & F University, Hangzhou 311300, China (e-mail: jiangxq@zafu.edu.cn; dhqzafu@163.com; hangis2002@163.com; wangyirong@stu.zafu.edu.cn).

Song Gao is with the College of Civil Engineering, Hunan University, Changsha, Hunan 410082, China (e-mail: gsong09@163.com).

Shenghui Fang and Yan Gong are with the School of Remote Sensing and Information Engineering, Wuhan University, Wuhan 430079, China (e-mail: shfang@whu.edu.cn; gongyan@whu.edu.cn).

Color versions of one or more of the figures in this article are available online at http://ieeexplore.ieee.org

I. INTRODUCTION

RICE is one of the major staple crops for humanity, feeding more than half of the world's population [1], [2], with its cultivation area exceeding 12% of the Earth's arable land [3]. Meanwhile, rice cultivation consumes a considerable amount of water resources [4], [5] and emits significant greenhouse gases, methane [6]. Therefore, timely and accurate spatial distribution maps of paddy rice are crucial for assessing food supply security, environmental protection.

Traditional approaches to monitoring rice cultivation area primarily rely on field surveys, which are time-consuming, labor-intensive, highly susceptible to human interference, and unable to achieve rapid and accurate large-scale monitoring [7]. Numerous studies have confirmed that remote sensing technology provides an accurate, rapid, and low-cost technical approach for paddy rice mapping [1], [8]. Optical images are the most widely used data source for paddy rice mapping due to their advantages of abundant satellite resources, rich spectral information and large information-carrying capacity. However, optical images are subject to cloud contamination, and the area under cloud coverage is equivalent to the blind spot of information, which results in the loss of valuable data. This is particularly detrimental during critical phenological stages for rice, such as the transplanting stages, significantly impacting the accuracy of paddy rice mapping. The International Satellite Cloud Climatology Project Flux Dataset (ISCCP-FD) estimates the global annual average cloud cover to be approximately 66% [9]. Due to the growth habits and environmental requirements of rice, critical phenological stages of rice are often distributed in cloudy and rainy seasons, making optical images of rice cultivation areas more susceptible to cloud contamination [10]. Therefore, cloud contamination poses a significant challenge for paddy rice mapping based on optical images.

To compensate for the loss of optical image data caused by cloud contamination, synthetic aperture radar (SAR) images, which can penetrate through clouds, have become an effective supplement to optical data sources. Numerous scholars have developed various methods solely utilizing SAR features for rice mapping [11], [12], [13]. For example, Zhan et al. [14] mapped rice fields using key "V" shaped feature in the Sentinel-1A VH backscatter time series before and after the rice transplanting stages. Xu et al. [15] proposed a SAR-based Paddy Rice Index (SPRI) for rice field identification. Previously, the authors [16] proposed an automatic rice

mapping method based on constrained feature matching (CFM classifier) for arbitrary length time series, improving the accuracy of rice mapping based on SAR features. However, due to the limited number of channels and relatively low signal-to-noise ratio of SAR images, the accuracy of paddy rice mapping based on SAR features still lags behind that based on spectral features under the same classifier [10]. In most regions, some optical images at different times are locally covered by clouds, with cloud-contaminated pixels accounting for a certain proportion in different images. Nonetheless, optical images still contains regions with less cloud coverage, indicating that a significant portion of optical images remains valuable [17]. Therefore, integrating optical and SAR features to leverage their respective advantages is a more reasonable approach for selecting remote sensing features in rice mapping. The accurate registration of SAR and optical images is the foundation for their effective fusion and the acquisition of complementary information, directly affecting the spatial detail representation of the fused image and the rice mapping accuracy. The differences in the imaging geometric models between the two types of images, along with issues such as speckle noise and geometric distortion in SAR images, present significant challenges to precise image registration [18], [19]. Currently, the precise registration technologies for SAR images have been greatly improved, laying the foundation for innovations in optical and SAR image fusion methods and the large-scale application of fused images [20], [21].

In the field of crop mapping, the fusion methods of optical images and SAR images mainly focus on pixel-level fusion, feature-level fusion, and decision-level fusion [22]. (i) Pixel-level fusion involves integrating optical and SAR image pixels through methods like wavelet transform, HIS transform, etc., to endow the fused pixels with information from both types of images [23]. Pixel-level fusion is usually for single-temporal images, which can improve classification accuracy under clear-sky conditions but may perform worse than using SAR images alone under cloudy conditions [24]. (ii) Feature-level fusion merges optical features with SAR features for classification. This type of fused data is often combined with machine learning methods for crop mapping, which is the most commonly used and has proven to be more effective [25], [26]. To avoid cloud contamination on data, the current conventional approaches are mostly to discard optical images with cloud coverage more than a certain percentage (e.g., 10%~15%) and then fuse the remaining optical images with SAR images for rice mapping [27], which significantly reduces the utilization of spectral features and causes some waste of optical images. (iii) At the decision-level fusion, optical and SAR data are utilized separately for rice mapping. By employing methods such as weighted voting and intersection, the classification results from both data sources are comprehensively considered to generate the final rice distribution map [28]. Currently, there is a lack of systematic research on how different cloud coverage percentages affect the accuracy of rice mapping under various remote sensing data fusion methods. Under cloud pollution conditions, which fusion method, feature-level or decision-level fusion, is more effective for rice mapping lacks scientific comparison and demonstration.

To address these problems, we propose an automatic decision-level fusion rice mapping method of optical and SAR images based on cloud coverage (the Auto-OSDF method). This method constructs evaluation indices to quantify the degree and spatial distribution of cloud contamination in optical images, and uses these indices as the basis for decision-level fusion of optical and SAR images. Using Bayesian optimization algorithms, the method drives the integration of the ITSGBT classifier with optical images and the CFM classifier with SAR images to conduct rice mapping experiments under varying cloud contamination levels. This process yields the optimal threshold space composed of the aforementioned evaluation indices. Finally, decision-level fusion is performed on the rice mapping results based on optical and SAR features. The objectives of this paper are: 1) to fully utilize clear-sky pixel information in cloud-contaminated optical images and leverage the advantages of SAR features in heavily cloud-polluted regions; 2) to achieve stable and accurate large-scale rice mapping under cloud coverage; 3) to ascertain the impact of different fusion methods of optical and SAR images on the accuracy of rice mapping. To validate the accuracy of rice mapping under cloud contamination, we first analyze the impact of different cloud coverage levels (10%~50%) on the accuracy of rice mapping based on the Auto-OSDF method, and then validate its value in large-scale application through rice mapping in Hunan Province. This research offers the following principal contributions:

1) This article proposes an automatic decision-level fusion rice mapping method for optical and SAR images. The method uses the degree of cloud contamination on individual optical pixels in the time series dimension as the basis for decision-level fusion of optical and SAR features, complementing clear-sky pixels with SAR images, thereby effectively mitigating cloud interference and achieving stable, high-precision rice mapping.
2) We propose a Bayesian optimization-based method to automatically obtain the threshold space for optimal fusion of optical and SAR images, maximizing the use of cloud-free optical features in cloudy images. The threshold space consists of three evaluation indices related to cloud contamination spatial distribution, designed to assess the absence and availability of optical features in the time series dimension.
3) This article systematically studies the impact of cloud coverage proportions on rice mapping accuracy using decision-level and feature-level fusion of optical and SAR data. As far as we know, it is the first quantitative and systematic study on how cloud coverage affects rice mapping accuracy and the effectiveness of fusion methods in mitigating cloud contamination.

II. STUDY AREA AND DATA

A. Study area

Hunan Province (108°47′~114°15′E, 24°38′~30°08′N) was chosen to assess the performance of the proposed Auto-OSDF method in large-scale applications. And Xiangyin County (112°30′20"-113°01′50"E, 28°30′13"-29°03′02"N) in Hunan Province was selected as the study area to analyze the impact of different cloud coverage levels on the accuracy of rice mapping.

Hunan Province is located in the middle reaches of the Yangtze River, and is close to Dongting Lake (Fig.1). It covers a total area of approximately 211,800 square kilometres. Hunan Province has subtropical monsoon climate, with an annual average temperature of 16~18 ℃ and abundant annual average precipitation of 1200 ~ 1800 mm. Hunan Province is an important grain production base in China, with main crops including rice, corn, soybeans. Rice mainly includes single-cropped rice (SCR) and double-cropped rice (DCR). The middle rice in the figure represents SCR, and the DCR contains both early rice and late rice. The medium rice is transplanted at the end of May or early June and harvested at the end of September. The early rice of DCR is transplanted in early or mid-April and harvested at the end of July, and the late rice is transplanted at the end of July and early August and harvested in mid- to late November. The crop calendars for major crops is shown in Fig. 2.

Xiangyin County is located in the northeastern part of Hunan Province, with a total land area of 1,541.45 square kilometres, and adjacent to Dongting Lake in the north. Rice, soybeans and corn are its main grain crops, and the rice cultivation areas are a mixture of SCR and DCR.

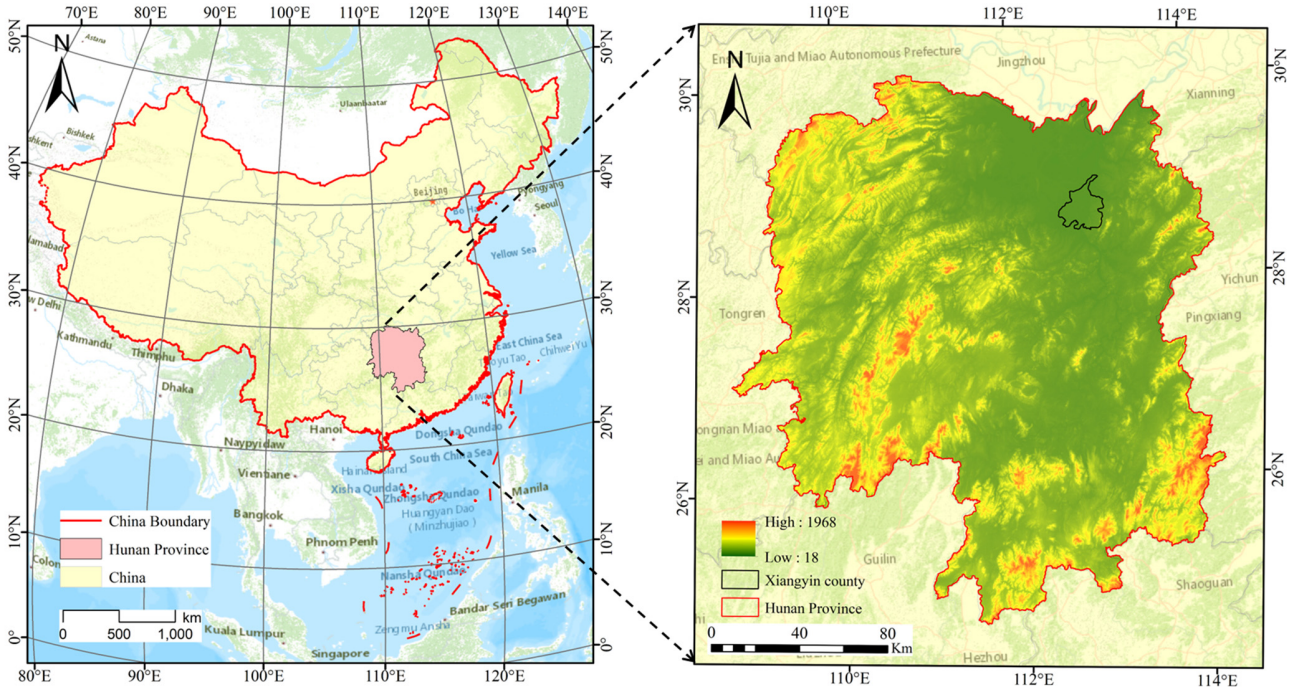

Fig.1. The location and topography of Hunan Province in China, as well as the location of Xiangyin County within Hunan Province.

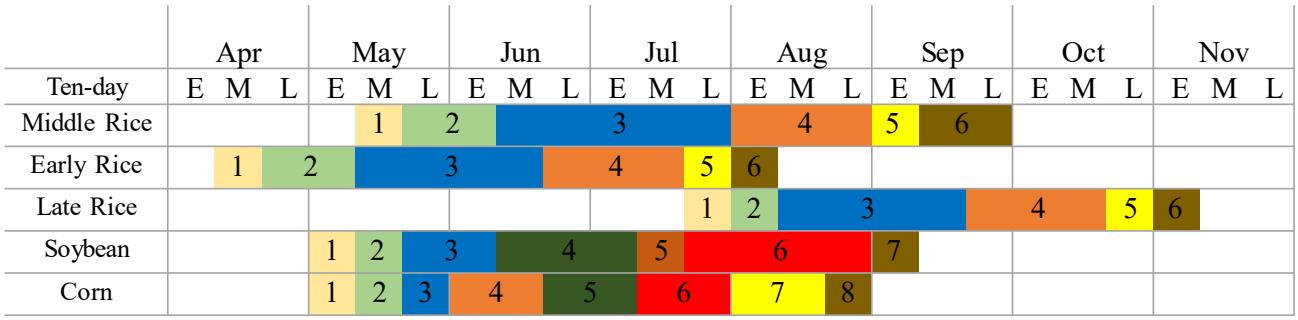

Fig.2. The crop calendar of main crops in Hunan Province.
Middle Rice: 1-Sowing, 2-Transplanting/flooding, 3-Tillering, 4-Heading, 5-Milky maturity, 6-Harvesting
Early Rice: 1-Sowing, 2-Transplanting/flooding, 3-Tillering, 4-Heading, 5-Milky maturity, 6-Harvesting

Late Rice: 1-Sowing, 2-Transplanting/flooding, 3-Tillering, 4-Heading, 5-Milky maturity, 6-Harvesting
Soybean:1-Sowing, 2-Seeding, 3-The third true leaf, 4-Braches forming, 5-Flowering, 6-Pod setting, 7-Harvesting
Corn: 1-Sowing, 2-Seeding, 3-Three leaves, 4-Seven leaves, 5-Sten elongation, 6-Heading, 7-Milky mature, 8-Harvesting

B. Data and processing

1) GF-6 data and Sentinel-1/2 data: The GF-6 wide-field view (WFV) datasets with a revisit cycle of 4-day and a spatial resolution of 16m were obtained from the China Resource Satellite Applications Centre (CRASAC). The GF-6 data has 8 spectral bands, including 2 red-edge bands that are sensitive to the chlorophyll content of plants.

Together Sentinel-2A and Sentinel-2B observe the earth's land surface with a repeat cycle of 5 days and a spatial resolution of 10-60 meters. Sentinel-2A/B MSI data has the advantage of higher spatial resolution（10m, 20m, 60m）and provide 13 spectral bands, including 3 red-edge bands. We selected Sentinel-1A GRD IW mode data with the spatial resolution of 10 m and the temporal resolution of 12 days. The vertical transmit/horizontal receive (VH) band which have been widely used for rice mapping was selected in this paper. All Sentinel datasets were obtained from the Copernicus Data Center of the European Space Agency (ESA). All images were selected from January 1, 2021 to December 31, 2021 and cover the entire study area, were downloaded from Copernicus Open Access Hub (https://scihub.copernicus.eu/dhus/#/home).

The Sentinel-1 datasets are preprocessed in Sentinel Applications Platform (SNAP) 6.0.0 and Python 3.8.2 versions using the following steps: apply orbit file, thermal noise removal, radiometric calibration, Refined Lee filter and Savitzky-Golay (SG) filter for filtering, Range-Doppler Terrain Correction combined with the Shuttle Radar Topography Mission (SRTM) digital elevation model, and the backscatter coefficients were transformed to dB. All Sentinel-2 MSI and GF-6 WFV datasets are preprocessed in ENVI 5.3 with the following steps: radiometric calibration, atmospheric correction, orthographic correction and geometric correction.

2) Reference data: To validate the reliability of the rice mapping method proposed in this study, two types of reference data were used: field survey data and agricultural statistics.

Field survey data was collected in May and September 2021. During the survey, we recorded the coordinates of different land cover types using GPS, and collected samples of various land cover types. To address the issue of some samples being located outside or at the edges of the plots, and some samples being too densely distributed, we combined the field survey samples with Google high-resolution images to regenerate the polygonal areas of regions of interest (ROIs), and then selected samples within the ROIs. During the field survey, we generally marked and located larger and more concentrated plots (typically at least 20×20m). For farmland, we entered the plot and located it at a certain distance from its boundaries. For inaccessible plots, such as water bodies, buildings, or certain farmlands, we located their outlines at the plot boundaries. However, when drawing ROIs with the aid of Google high-resolution images, the ROI outlines were controlled within the on-site located plot boundaries to avoid mixed pixel issues at the edges. The Sentinel-2 image closest to the survey date was selected as the base map, with only the pixels inside the ROIs marked as valid samples, while the pixels on the boundary of the ROIs were excluded. These samples were distributed evenly throughout the entire study area, as shown in Fig. 3. The number of sample data points obtained from the field survey and Google Earth for the entire Hunan Province and the Xiangyin County is shown in Table I.

TABLE I
THE NUMBER OF SAMPLES FOR THE LAND COVER TYPES FOR THE ENTIRE HUNAN PROVINCE AND THE XIANGYIN COUNTY

Land cover type	Hunan Province	Xiangyin County
Single rice	23709	2359
Double rice	13150	2157
Corn	2936	835
Soybean	3564	912
Water	16947	2360
Forest	14697	2040
Building	11076	2800
Sum	86079	13463

The rice planting statistics data was collected from the provincial and prefectural statistical yearbook of Hunan Province in the year of 2022. Specifically, a total of 14 prefecture-level cities in Hunan Province was used for accuracy assessment of rice planting maps. The rice planting statistics data in statistical yearbook was obtained through sample surveys.

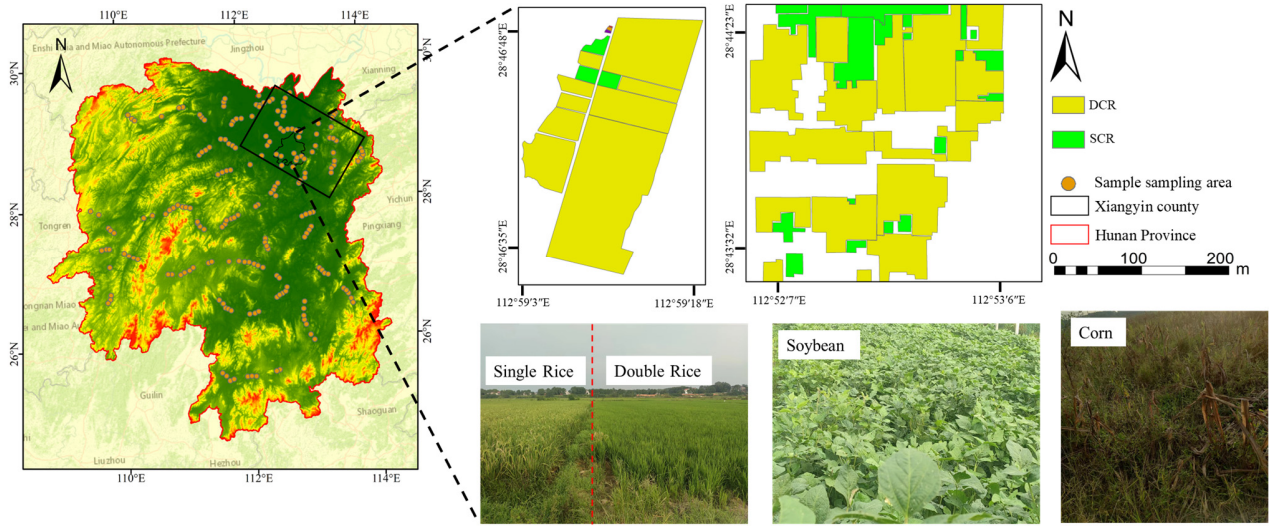

Fig. 3. Location of the sample collection points in Hunan Province and field photos of different land covers

III. METHODOLOGY

A. Overview of the Auto-OSDF method

In this paper, an Auto-OSDF method was proposed for large-scale rice mapping in cloud-contaminated regions, which includes a novel classifier module for time-series remote sensing data, an assessment module for cloud contamination of optical images, and an optimal threshold space auto-acquisition module. The schematic diagram of the method is shown in Fig. 4. The classifier module (detailed in Section III-D) includes the CFM classifier [16] and the ITSGBT classifier [29] proposed by the authors previously. They respectively combine SAR and optical images for rice mapping, offering distinct advantages.

The method incorporates cloud coverage and its spatial distribution detection, automatic threshold space acquisition, feature and classifier selection, and decision-level fusion into a unified framework. Specifically, the pixel data at any position in the time-series optical image T is denoted as t_{ij}, the evaluation indices of cloud contamination spatial distribution (CPL indices) are represented by Z, and the threshold space obtained by the optimal threshold space auto-acquisition module is denoted by Ω. This method first obtains the CPL indices $Z^{t_{ij}}$ for the pixel at position t_{ij} through the assessment module for cloud contamination of optical images, evaluating the cloud pollution of that pixel in the time-series dimension. If $Z^{t_{ij}}$ falls within the threshold space Ω, it indicates that the pixel has a lighter degree of cloud pollution, and thus, the pixel is classified using the ITSGBT classifier combined with optical images for land cover type identification. If $Z^{t_{ij}}$ falls outside the Ω, it indicates a heavier degree of cloud pollution and significant loss of valid information; therefore, the pixel is classified using the CFM classifier combined with SAR image. Finally, the final decision-level fusion of the above classification results yields the ultimate rice distribution map. The decision of which classifier to use for land cover type identification for each pixel data at position t_{ij} is determined by Eq. (1).

$$f^{t_{ij}} = \begin{cases} f^{t_{ij}}_{ITSGBT}, & Z^{t_{ij}} \in \Omega \\ f^{t_{ij}}_{CFM}, & Z^{t_{ij}} \notin \Omega \end{cases} \tag{1}$$

where $f^{t_{ij}}$ represents the land cover type identification result for pixel t_{ij}, $f^{t_{ij}}_{ITSGBT}$ represents the land cover type identification result for pixel t_{ij} using the ITSGBT classifier combined with optical images, and $f^{t_{ij}}_{CFM}$ represents the land cover type identification result for pixel t_{ij} using the CFM classifier combined with SAR images.

Additionally, this paper proposes an optical image quantitative proportion cloud mask random generation (QPCM) algorithm. The algorithm can randomly generate cloud masks at quantitative proportions in optical images, which are used to test the effectiveness of the Auto-OSDF method proposed in this paper under different cloud coverage proportions, as detailed in Section III-E.

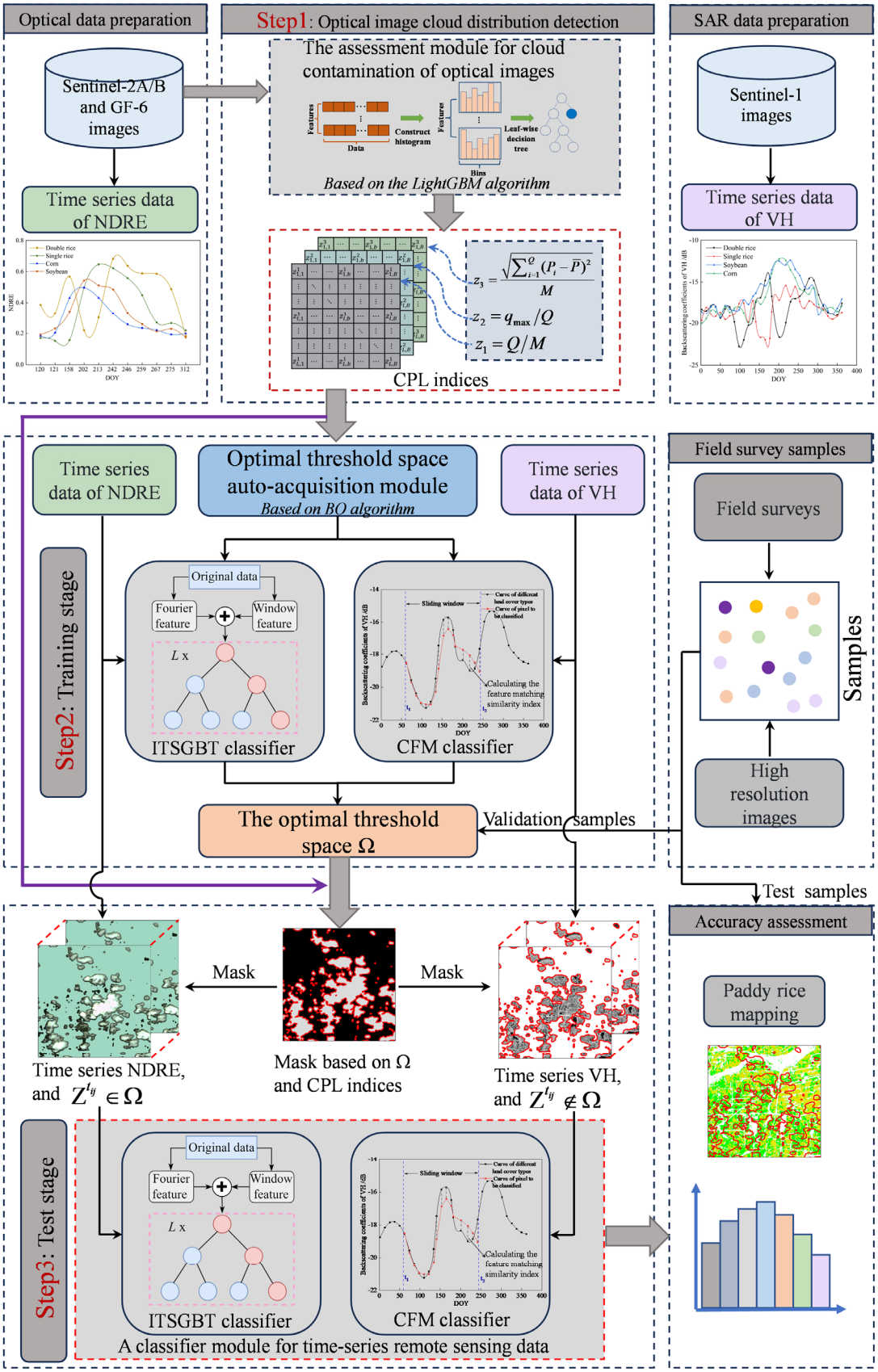

Fig. 4. The schematic diagram of the Auto-OSDF method

B. The assessment module for cloud contamination of optical images

High-precision cloud detection is crucial for quantitatively evaluating the influence of cloud contamination on pixels, and it is also a prerequisite for efficiently utilising less cloud-contaminated optical images in this paper. The assessment module for cloud contamination of optical images can perform continuous fast cloud detection, create cloud masks, and automatically locate cloud coverage regions on GF-6 and Sentinel-2 time series images. It can also statistically analyze the cloud coverage proportion and the CPL indices. Inspired by the S2cloudless cloud detection model, the cloud detection function of this module is implemented using the lightGBM algorithm [30], [31].

The total number of periods in the time series optical images is M, for any optical image pixel at position t_{ij}, the assessment module can automatically detect and mark the number of periods Q affected by cloud contamination, as well as the positions P_k (k=1,…,Q) of the cloud-contaminated images in the time series. It then calculates three CPL indices for each pixel as follows:

1) Cloud Occurrence Frequency (z_1): The ratio of the number of cloud-contaminated periods to the total number of periods, which is

$$z_1 = Q/M \tag{2}$$

This indicates how often the pixel is affected by clouds over the entire time series.

2) Cloud Persistence (z_2): The proportion of the maximum continuous cloud-contaminated period number q_{max} for a single pixel to the total number of cloud-contaminated periods Q, which is

$$z_2 = q_{\max}/Q \tag{3}$$

This indicates how long cloud coverage typically persists over the pixel.

3) Cloud Dispersion (z_3): The dispersion degree of cloud-contaminated positions P_k in the time series, which is

$$z_3 = \frac{\sqrt{\sum_{i=1}^{Q}(P_i - \bar{P})^2}}{M} \tag{4}$$

This reflects how evenly or unevenly cloud contamination is spread across the time series for that pixel.

C. The optimal threshold space auto-acquisition module

The CPL indices mentioned above, namely the cloud occurrence frequency z_1, the cloud persistence z_2, and the cloud dispersion z_3, can reflect the absence degree of optical features in time series dimension affected by cloud contamination. They are also closely related to the classification accuracy based on optical features. Therefore, the optimal threshold space Ω for these CPL indices, represented as [δ_1, δ_2, δ_3], is set as the decision condition for the Auto-OSDF method to select optical features or SAR features, as well as ITSGBT classifier or CFM classifier. The optimal threshold space Ω is automatically obtained through the Bayesian optimization (BO) algorithm, following the principle that the average overall accuracy of classification for different cloud coverage proportions is maximized in the validation set. In this paper, the probabilistic surrogate model selects the Gaussian process, and the acquisition function selects the upper confidence bound function. The Bayesian optimization algorithm can seek the optimal value of the function by constructing a black-box function and continuously updating the posterior distribution of the objective function with new sample points under the condition of limited sample points. The process of seeking the threshold space Ω can be transformed into an optimization problem as follows:

$$\Omega = \arg\max_{z \in Z} f(z) \tag{5}$$

where the objective function f(z) is the average of the overall accuracy.

D. A classifier module for time-series remote sensing data

The classifier module includes the CFM classifier [16] and the ITSGBT classifier [29] proposed by the authors previously.

The CFM classifier includes a feature matching similarity index that considers both the overall and local shape differences of the time series curve. The aforementioned shapes of the time series feature curves are closely related to the crop phenology characteristics. It adopts dynamic sliding matching technology to seek the optimal matching of the time series curves, thereby accounting for phenological differences caused by factors such as varying rice planting times between different parcels. By setting constraint parameters, it reduces the interference from non-vegetation land cover types on the rice mapping. This classifier is applicable to time series curves of arbitrary lengths, overcoming the issue of inconsistent lengths caused by partial image absence. The technical scheme of this classifier is meticulous and can fully exploit the local and overall shape features of the time series curves. However, when faced with a large numbers of feature types, determining the constraint parameters becomes challenging. Therefore, this classifier is particularly well-suited for processing SAR images, as they have fewer channels and the channel information is closely related to rice phenology. Preliminary experimental research has also demonstrated that this classifier achieves better rice mapping accuracy compared to traditional machine learning methods when combined with SAR features [16].

The ITSGBT classifier is specifically designed for time-series remote sensing data to extract the local and overall shapes of curves from multiple time-series curves. In this classifier, the time series curves are first split into numerous subsequences by random intervals, and interval features, including the mean, standard deviation, and linear least squares fitting slope, are extracted from each subsequence. Then, the Fourier coefficients of the time series curves are

extracted via DFT. Finally, the pipeline mechanism is used to combine, the automatic acquisition of the above features and the gradient boosting tree classification, into a unified model framework for rice mapping. The ITSGBT classifier is well-suited for handling various types of long time-series features, and its computational efficiency does not significantly decrease with an increase in feature types and time series length. Therefore, this classifier can leverage the advantages of optical images with many channels, rich spectral and vegetation index information. Preliminary experiments have also shown that when combined with optical images, this classifier can improve the accuracy of rice mapping compared to conventional machine learning classifiers [29].

E. The optical image quantitative proportion cloud mask random generation (QPCM)algorithm

To quantitatively evaluate the impact of different cloud coverage on the rice recognition accuracy by the Auto-OSDF method, an QPCM algorithm is proposed for accurately controlling the proportion of cloud-contaminated pixels in optical images. The overall idea of the algorithm is:

1) Detecting the proportion of cloud contamination in all images using the optimal threshold space auto-acquisition module.

2) If the cloud contamination proportion is less than the set cloud proportion, a cloud mask is randomly generated in images by expanding with Exr as the expansion radius on the basis of a square with side length SL.

3) Compare the generated cloud mask with the set cloud ratio, if there remain differences, then adjust the cloud size until the difference between the generated cloud mask and the set cloud proportion is less than the set value (the set value in this paper is 0.01%)

This quantitatively proportional cloud mask random generation algorithm for optical images has the following characteristics: a) The proportion of cloud pixels can be precisely controlled for all optical images; b) the cloud masks for all optical images are randomly generated, which is also because the distribution of clouds in nature is also arbitrary.

IV. EXPERIMENT

A. Experimental setup

We will verify the accuracy of the Auto-OSDF method proposed in this paper for rice recognition under cloud contamination through two stages of experiments, as shown in Table II. In the first stage, Xiangyin County in Hunan Province is taken as the study area. The experiment quantitatively controls the proportion of cloud coverage in optical images through the proposed QPCM algorithm. The cloud coverage proportion of each optical image in this experiment is set to 10%, 15%, 20%, 25%, 30%, 35%, 40%, 45%, and 50%, respectively, to analyze the impact of different cloud coverage proportion on the accuracy of rice mapping based on the Auto-OSDF method, referred to as Experiment 1. The Auto-OSDF method is a decision-level fusion method of optical features and SAR features. Furthermore, to compare the advantages and disadvantages of the feature-level fusion of optical features and SAR features under different cloud coverage proportion, Experiment 2 uses the ITSGBT classifier combined with optical images (hereinafter referred to as ITSGBT-OI), while Experiment 3 uses the ITSGBT classifier combined with optical and SAR feature-level fusion features (hereinafter referred to as ITSGBT-OSI). Experiment 2 can illustrate the impact of different cloud coverage proportion on the accuracy of rice mapping using only optical features. Experiment 3 can illustrate the impact of different cloud coverage proportion on the accuracy of rice mapping using optical and SAR combined features (i.e., fusion at the feature level). The specific approach of feature-level fusion is to directly overlay optical features with SAR features, which is equivalent to taking the union of the two types of features, and using the combined features as the input to the classifier. In the second stage, the entire Hunan Province is taken as the study area. Based on the Auto-OSDF method, the rice fields of the entire Hunan Province are mapped and compared with the ground truth data to validate the value of the proposed method in large-scale applications. This is referred to as Experiment 4.

TABLE II
THE SPECIFIC EXPERIMENTAL SCHEME IN THIS PAPER

Experiment number	Rice mapping method	Classifier	Satellite data	Fusion methods	Study site
Experiment 1	Auto-OSDF	CFM classifier and ITSGBT classifier	GF-6, Sentinel-2A/B and Sentinel-1	Decision-level fusion	Xiangyin County
Experiment 2	ITSGBT-OI	ITSGBT classifier	GF-6 and Sentinel-2A/B	Only optical images, no fusion	Xiangyin County
Experiment 3	ITSGBT-OSI	ITSGBT classifier	GF-6, Sentinel-2A/B and Sentinel-1	Feature-level fusion	Xiangyin County
Experiment 4	Auto-OSDF	CFM classifier and ITSGBT classifier	GF-6, Sentinel-2A/B and Sentinel-1	Decision-level fusion	Hunan Province

The above-mentioned optical image data sources select the Normalized Difference Red Edge (NDRE) features from GF-6 and Sentinel-2, and the SAR data source is the VH channel features from Sentinel-1.

Previous studies [32], [33] have shown that red-edge vegetation indices constructed from red-edge bands and near-infrared bands, such as the normalized difference red edge (NDRE), can improve crop classification accuracies.

Therefore, NDRE was chosen as the input feature for all the experiments. The NDRE can be expressed as:

$$NDRE = \frac{\rho_{NIR} - \rho_{red-edge}}{\rho_{NIR} + \rho_{red-edge}} \quad (6)$$

where ρ_{NIR} and $\rho_{red-edge}$ are the reflectances corresponding to the near-infrared band, and the red-edge band, respectively.

The samples are divided into three parts: training set, validation set, and test set. The proportions of the above sets are 40%, 40%, and 20%, respectively. Each category of land cover in TABLE I is assigned to different datasets according to the aforementioned ratio ensure the uniformity of the dataset for each land cover category as much as possible. Experiments 1 to 3 focus on Xiangyin County as the study area, thus only using samples from Xiangyin County to train different classifiers. Experiment 4 considers the entire Hunan Province as the study area, so samples from the entire province are used. Furthermore, when dividing the sample dataset for the entire Hunan Province, we conduct uniform sampling within each municipal administrative region to guarantee that the samples are evenly distributed across the entire area, ensuring regional representativeness.

The complete training and evaluation process of the Auto-OSDF model in both Experiment 1 and Experiment 4 can be divided into the following three steps: (i) Train the ITSGBT classifier based on the training set and determine the optimal hyperparameters according to its performance on the validation set. Simultaneously, select the optimal threshold based on the accuracy of the CFM classifier on the validation set. (ii) In the validation set, use a Bayesian optimization method to drive the optimal CFM classifier and ITSGBT classifier obtained in the first step, with the principle of maximizing average overall accuracy for rice mapping under different cloud coverage proportion, to quickly obtain the optimal threshold space Ω composed of CPL indices. (iii) Apply the well-trained Auto-OSDF model to the test set for accuracy evaluation. The above training and evaluation processes are executed automatically through a pipeline mechanism.

Overall accuracy (OA) and Kappa coefficient are used as quantitative evaluation indicators for the effectiveness of different methods in all experiments.

B. Experimental results

1) The impact of cloud coverage proportion on the accuracy of rice mapping based on ITSGBT-OI (Experiment 2): To make the differences in the results of rice mapping based on ITSGBT-OI under varying cloud coverage ratios more evident, only the rice distribution maps and locally magnified maps for Xiangyin County at cloud coverage proportions of 10%, 20%, 30%, 40%, and 50% are presented, as shown in Fig. 5. From Fig. 5, it can be observed that rice is quite widely distributed in Xiangyin County, mainly in the southern and western parts. Due to Dongting Lake in the north, mountainous terrain in the east, and plains in the southwest, rice is most extensively distributed in the southwest.

From Fig. 5, the overall trend of increasing misclassification and gradually more noise is observed with increasing cloud coverage. Under 10% cloud coverage, the misclassification and noise of rice field maps are relatively low, and the boundaries between parcels are relatively clear and regular (Fig. 5(a)(f)). Under 20% cloud coverage, there is an increase in the misclassification of rice field maps, accompanied by heightened noise within the parcels and greater irregularities in parcel boundaries (Fig. 5(b)(g)). Under cloud coverage ratios of 30% to 50%, misclassification and noise increase as cloud coverage increases, with more obvious misclassification between SCR and DCR (Fig. 5 (c) (h) (d) (i) (e) (j)).

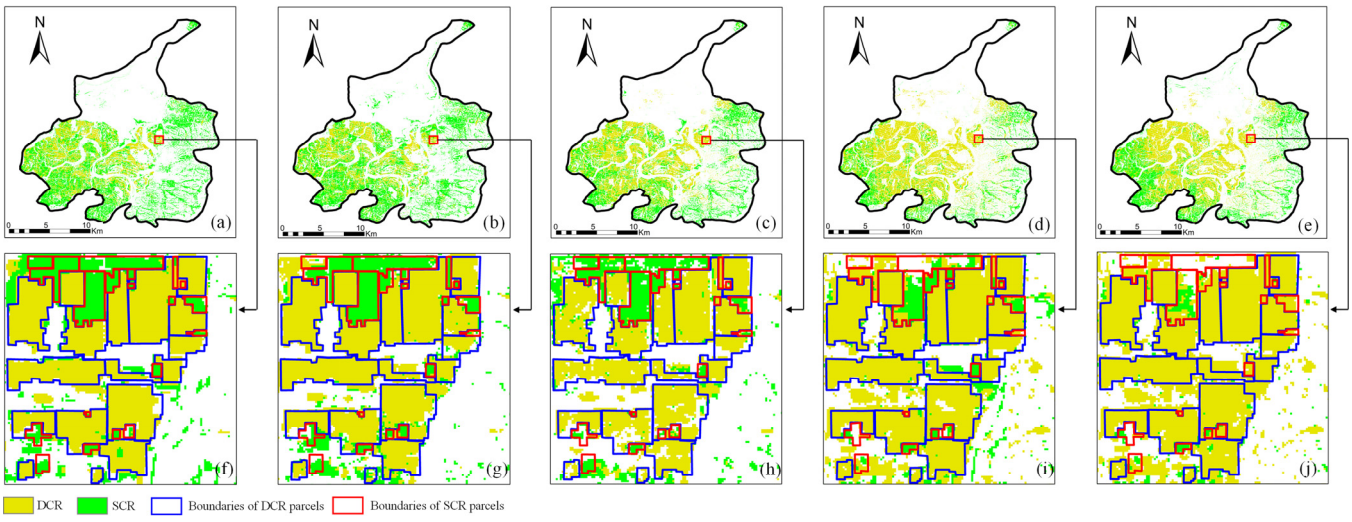

Fig. 5. Rice distribution maps and locally magnified maps for Xiangyin County based on ITSGBT-OI under different cloud coverage: (a)(f) Under 10% cloud coverage; (b)(g) Under 20% cloud coverage; (c)(h) Under 30% cloud coverage; (d)(i) Under 40% cloud coverage; (e)(j) Under 50% cloud coverage.

Figure 6 shows the trend of OA and Kappa coefficient based on ITSGBT-OI with varying cloud coverage. It can be seen that as cloud coverage increases, the OA and Kappa coefficient gradually decrease. Under 10% and 20% cloud coverage, the OAs are both above 95%, with Kappa coefficients of 0.93 and 0.92 respectively. This indicates that under cloud coverage below 20%, the method can accurately identify rice, and the impact on rice mapping accuracy based on ITSGBT-OI is not very significant, hence special processing for cloud-contaminated pixels is not necessary. Under 30% cloud coverage, the OA of rice field maps decreases to 90.03%, with a Kappa coefficient of 0.85, showing a significant decrease in accuracy, indicating the need to consider the impact of cloud contamination on rice mapping accuracy. With further increase in cloud coverage, the speed of decrease in rice mapping accuracy also accelerates.

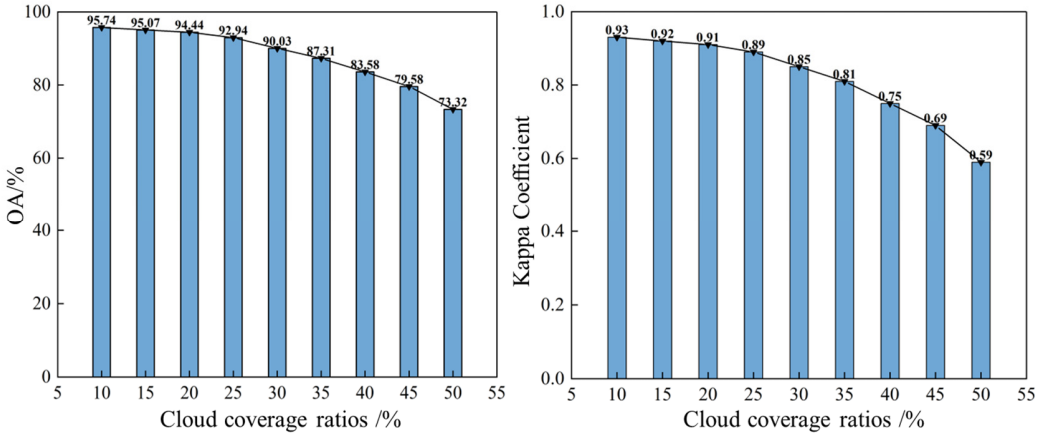

Fig. 6. Evaluation results of rice mapping accuracy based on the ITSGBT-OI under different cloud coverage ratios: (a) Overall Accuracy; (b) Kappa Coefficient.

2) The impact of cloud coverage proportion on the accuracy of rice mapping based on ITSGBT-OSI (Experiment 3): Figure 7 shows the rice distribution maps and locally magnified maps for Xiangyin County obtained based on ITSGBT-OSI under cloud coverage proportions of 10%, 20%, 30%, 40%, and 50%. From Fig. 7, it can be observed that with the increase of cloud coverage, the overall trend of misclassification and noise increases. Under 10% cloud coverage, there are relatively few misclassifications of rice field maps, with slightly more noise compared to using only optical data, which is related to the inherent noise in SAR data (Fig. 7 (a) (f)); Under 20% and 30% cloud coverage, the misclassification of rice field maps increases, and the noise within the parcels further increases, leading to increased irregularity in the identified parcel boundaries (Fig. 7 (b) (g) (c) (h)); Under 40% and 50% cloud coverage, the misclassification of land cover types further increases, and the "salt-and-pepper noise" becomes more pronounced, with significantly increased irregularity in the identified parcel boundaries (Fig. 7 (d) (i) (e) (j)).

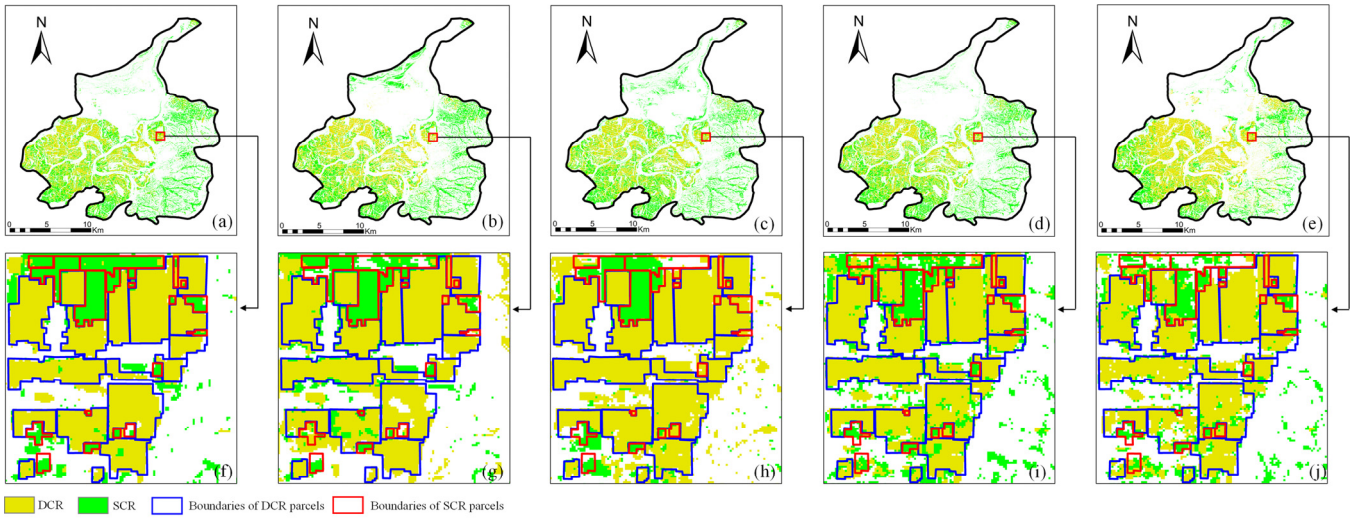

Fig. 7. Rice distribution maps and locally magnified maps for Xiangyin County based on ITSGBT-OSI under different cloud coverage: (a)(f) Under 10% cloud coverage; (b)(g) Under 20% cloud coverage; (c)(h) Under 30% cloud coverage; (d)(i) Under 40% cloud coverage; (e)(j) Under 50% cloud coverage.

Figure 8 shows the trend of OA and Kappa coefficient with varying cloud coverage based on ITSGBT-OSI. It can be seen that with the increase of cloud coverage, the OA and Kappa coefficient of rice gradually decrease. The OAs exceed 90% when the cloud coverage is below 25%. However, with the further increase of cloud coverage proportion, the rate of decrease in rice mapping accuracy also accelerates. In summary, compared to the ITSGBT classifier combined with optical images only, the ITSGBT classifier combined with optical and SAR feature-level fusion images improves the rice mapping accuracy at higher cloud coverage, but the OA decreases with the increase of cloud coverage, and it does not enable accurate rice mapping when the cloud coverage proportion is high.

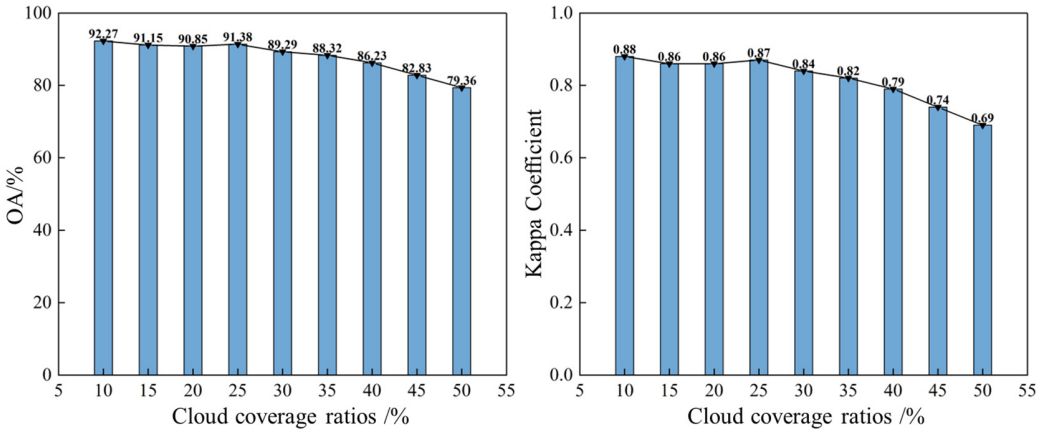

Fig. 8 Evaluation results of rice mapping accuracy based on the ITSGBT-OSI under different cloud coverage ratios: (a) Overall Accuracy; (b) Kappa Coefficient.

3) The impact of cloud coverage proportion on the accuracy of rice mapping based on Auto-OSDF (Experiment 3): Figure 9 depicts the rice mapping results based on the Auto-OSDF method at cloud coverage ratios of 10%, 20%, 30%, 40%, and 50%. It can be seen that with increasing cloud coverage, the overall rice mapping results based on the Auto-OSDF method remain relatively stable, without significant increases in misclassifications or noise. Under cloud coverage ratios of 10% to 30%, there are few misclassifications and less noise in the rice distribution maps, and the boundaries among parcels are clear and regular. The method can distinguish the SCR and DCR well, and it is able to map the fragmented parcels of rice accurately (Fig. 9 (a) (f) (b) (g) (c) (h)). However, under cloud coverage percentages of 40% and 50%, the local misclassification and noise in the rice distribution map increases slightly. Nevertheless, the extracted parcel boundaries remain relatively clear and regular (Fig. 9 (d) (i) (e) (j)).

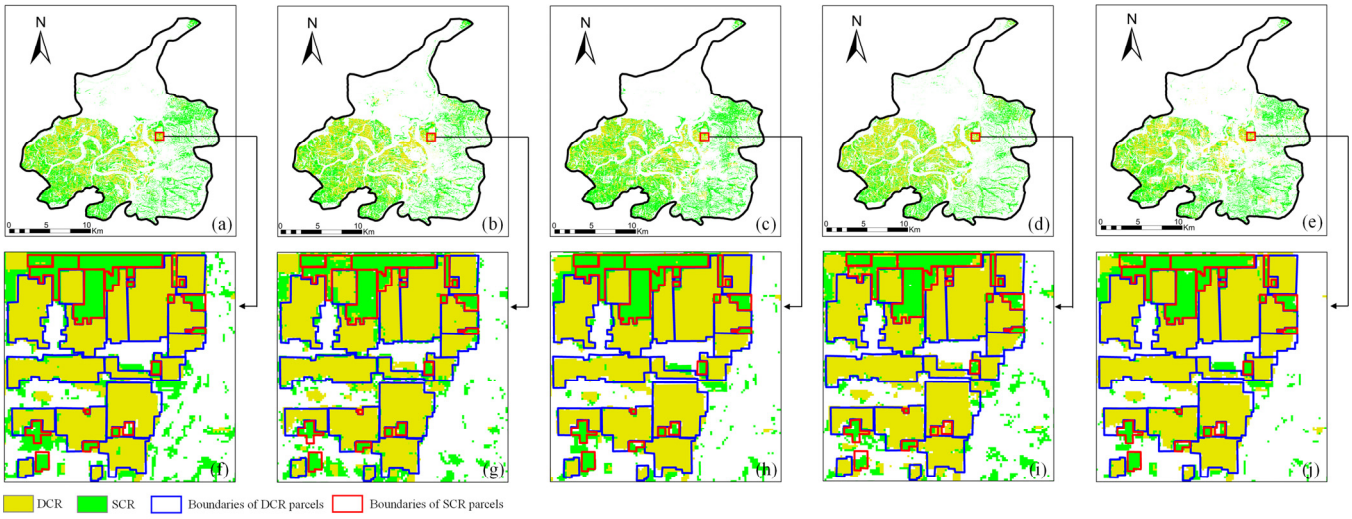

Fig. 9. Rice distribution maps and locally magnified maps for Xiangyin County based on the Auto-OSDF method under different cloud coverage: (a)(f) Under 10% cloud coverage; (b)(g) Under 20% cloud coverage; (c)(h) Under 30% cloud coverage; (d)(i) Under 40% cloud coverage; (e)(j) Under 50% cloud coverage.

Figure 10 illustrates the trend of OA and Kappa coefficients based on the Auto-OSDF method as cloud coverage varies. It can be observed that with increasing cloud coverage, the OA and Kappa coefficients remain relatively stable, with a slight downward trend. At cloud coverage percentages of 10%, 20%, and 30%, the OAs of the rice distribution map are 94.88%,

95.59%, and 95.18% respectively, with Kappa coefficients of 0.92, 0.93, and 0.92 respectively. From Fig. 10, it can be seen that when the cloud coverage ranges from 10% to 30%, the OA of the rice distribution map fluctuates around 95%. When the cloud coverage increases from 30% to 50%, there is a slight decrease in rice mapping accuracy, but the OA still exceeds 93%, indicating that even under severe cloud contamination, the method can realize high-precision rice mapping. This demonstrates the high accuracy and stability of the method under different levels of cloud contamination.

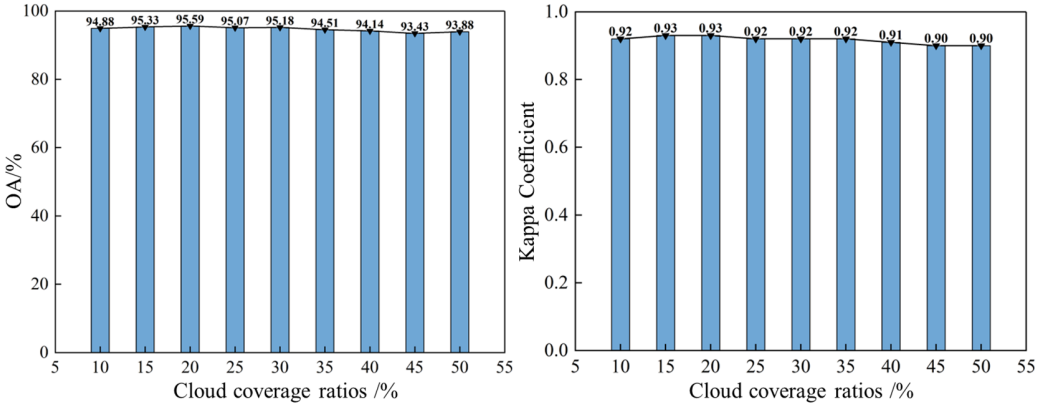

Fig. 10. Evaluation results of rice mapping accuracy based on the Auto-OSDF method under different cloud coverage ratios: (a) Overall Accuracy; (b) Kappa Coefficient.

4) Application of the Auto-OSDF method in the extraction of rice cultivation areas in Hunan Province (Experiment 4): Figure 11 depicts the rice distribution map of Hunan Province obtained based on the Auto-OSDF method. As shown in Figure 11, rice cultivation areas are widely distributed in Hunan Province, with a cultivation pattern that mixes SCR and DCR. DCR is mainly distributed in the northeastern part of Hunan Province, while SCR exhibits a more widespread distribution.

Compared with the field survey data, the OA of the rice mapping obtained through the Auto-OSDF method in Hunan Province is 92.47%, and the Kappa coefficient is 0.87. By using the rice distribution map combined with the pixel number approach, the rice planting area in Hunan Province is obtained and compared with the fourteen municipal agriculture statistics, as shown in Fig. 13. It can be observed that the results obtained by the Auto-OSDF method show an average R^2 value of 0.926 compared to municipal-level statistical planting areas. These results demonstrate the reliability and significant value of the method for large-scale rice mapping.

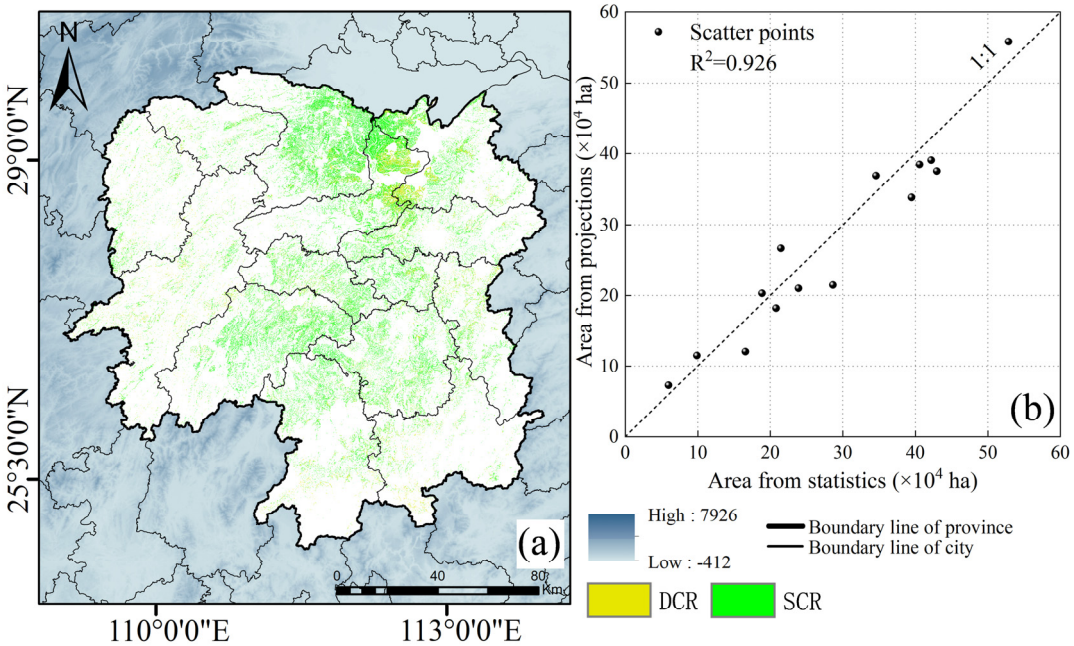

Fig. 11. The rice distribution map of Hunan Province based on the Auto-OSDF method and its accuracy evaluation: (a) the rice distribution map; (b) comparison of paddy rice planting area between the predicted results and official statistics.

V. DISCUSSION

A. Impact of different cloud coverage on the accuracy of various methods and analysis of the principles

For rice mapping based on ITSGBT-OI, cloud coverage of 20% or less does not significantly affect the accuracy of rice mapping. However, as cloud coverage increases further, the accuracy of rice mapping decreases more rapidly. This phenomenon occurs because when there are few clouds in each time period, the overlap in cloud locations between different periods is low. In other words, within a single pixel time series, the proportion of cloudy periods to the overall time series is not significant. Therefore, the impact of low cloud coverage on the accuracy of rice mapping is not very obvious. However, as cloud coverage increases, the proportion of cloud-containing periods within a single pixel time series increases. The shape characteristics of key phenological phases of rice may be obscured by clouds. This results in a decrease in the differences of the time series curves between rice and other crops. Therefore, the OA of rice mapping decreases rapidly with the increase in cloud coverage.

For rice mapping based on ITSGBT-OSI, when the cloud coverage ratio is between 10% and 25%, the overall accuracy of rice mapping can reach over 90%. However, as the cloud coverage ratio increases, the decline in rice mapping accuracy accelerated. As shown in Fig. 12, with the increase in cloud coverage, the decline in the accuracy of rice mapping using ITSGBT-OSI is slower than that based on ITSGBT-OI. When the cloud coverage is between 10% and 30%, the addition of SAR features does not always improve the accuracy of rice mapping. The main reason is that SAR images have their own noise, and the noise superimposed by cloud contamination has a certain impact on rice mapping accuracy. At the same time, due to the addition of SAR features, some feature information of land covers can be provided in areas with serious cloud contamination in optical images, which is also the reason why the decline in rice mapping accuracy based on ITSGBT-OSI is slower than that based on ITSGBT-OI as the cloud coverage ratio increases. The experimental results indicate that as cloud coverage increases, the improvement in rice mapping accuracy by fusing optical images with SAR images at the feature level is not significant (Fig. 8).

For rice mapping based on the Auto-OSDF method, when cloud coverage is between 10% and 30%, the overall accuracy of rice mapping still fluctuates around 95%; when cloud coverage is between 30% and 50%, the accuracy of rice mapping can still be maintained above 93% (Fig. 10). The experimental results show that as cloud coverage increases, the impact on the accuracy of rice mapping using the Auto-OSDF method is relatively small. The reason for the above experimental results is that when the cloud coverage is low, the ITSGBT classifier combined with time series optical images can already extract rice with high accuracy. As the cloud coverage increases, the proportion of cloud-containing periods within a single pixel's time series increases, and the presence of a large amount of cloud noise makes the differences in the time series optical characteristics between land covers smaller. Therefore, the probability of misclassification by the ITSGBT classifier using only time series optical images will greatly increase, leading to a decrease in the accuracy of rice mapping. In response to the above situation, when the CPL indices do not meet the threshold space Ω, the CFM classifier proposed by the author in previous studies is used in conjunction with SAR images for classification. Since the CFM classifier is specifically designed and optimized for time series SAR images, a pixel with a high proportion of cloud-containing periods can still maintain high accuracy after being classified with this classifier. That is, as cloud coverage gradually increases, the role of the CFM classifier combined with time series SAR images in the overall classification results gradually increases, and this classifier can also extract rice with high accuracy. The final rice mapping results use the classification results of the CFM classifier combined with SAR images in areas with severe cloud contamination, and use the classification results of the ITSGBT classifier combined with optical images in areas with cloud coverage, which can maintain high-precision rice mapping across the entire study area. Compared with the ITSGBT classifier combined with the fusion of optical and SAR features at the feature level, the Auto-OSDF method is more effective in addressing the impact of cloud contamination on the accuracy of rice mapping.

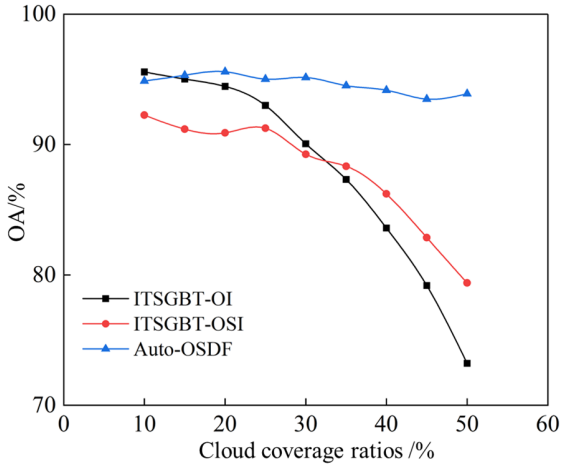

Fig. 12. Comparison of rice prediction accuracy of various methods under different cloud coverage ratios.

B. Selection of rice mapping methods under different cloud coverage proportions

When using the same samples, the rice mapping methods based on ITSGBT-OI and Auto-OSDF both achieve OAs exceeding 94% under cloud coverage ratios of 10% to 20%. Moreover, when the cloud coverage ratio is less than 10%, the OA of rice mapping based on ITSGBT-OI is higher than 95% (Fig. 6). This indicates that when the cloud coverage ratio is below 20%, rice mapping can be performed solely using the ITSGBT classifier combined with optical images, without the

need for fusion with SAR images. Previously, the CFM classifier proposed by the authors achieved an OA of 94.02% using only Sentinel-1 SAR images under the same samples at Study Site 1 [16]. However, in this study, when the cloud coverage ratio exceeds 20%, the accuracy of rice mapping based on ITSGBT-OI is lower than that of rice mapping based solely on SAR images. Therefore, in such cases, it is not advisable to map rice by only combining optical images. When the cloud coverage ratio is between 20% and 40%, the rice mapping accuracy based on the Auto-OSDF method is higher than 94%. Even when the cloud coverage ratio exceeds 40%, although the rice mapping accuracy decreases, the OA still approaches 94%, significantly higher than that based on ITSGBT-OI (Fig. 10). Additionally, the rice mapping accuracy does not significantly decrease with an increase in cloud coverage. In addition, the Auto-OSDF method only uses the classification results of the CFM classifier to replace the cloud-contaminated areas when the CPL indices of a single pixel do not meet the threshold space Ω, and Ω≠0, meaning that there is always a classification result of optical images with cloud noise involved in the final rice mapping. Therefore, when the cloud coverage exceeds a certain proportion (in this experiment, it is 40% cloud coverage), the rice mapping method using the CFM classifier solely with SAR images is superior to the Auto-OSDF method.

In summary, based on the experiments in this study, when the overall average cloud coverage of the time series optical images is less than 20%, it is recommended to use the ITSGBT classifier combined with optical images for rice mapping. When the cloud coverage is between 20% and 40%, the Auto-OSDF method is recommended for rice mapping. When the cloud coverage exceeds 40%, it is recommended to use the CFM classifier combined with SAR images for rice mapping (Fig. 12).

VI. Conclusion

An Auto-OSDF method is proposed in this paper for large-scale rice mapping in cloudy and foggy areas. The method achieves stable and high-precision rice mapping under cloud contamination by fusing optical and SAR features at the decision level and by leveraging the optical features of cloud-free pixels in cloudy images. Furthermore, this paper systematically studies the impact of different cloud coverage proportions on the accuracy of rice mapping based on the decision-level fusion of optical and SAR features, as well as the feature-level fusion. The Auto-OSDF method was applied in Xiangyin County, Hunan Province, to analyze the impact of varying cloud coverage levels (10% to 50%) on the accuracy of rice mapping. Then, to demonstrate the value of the proposed method in large-scale applications, we further mapped the rice fields of the entire Hunan Province. The following conclusions were drawn:

1) The accuracy of rice mapping based on the Auto-OSDF method is less affected by cloud contamination. The OA and Kappa coefficient under different cloud coverage proportions are all above 93% and 0.9, respectively, indicating that the method can perform high-precision rice mapping well in areas with varying cloud coverage levels.

2) The OA and Kappa coefficient of rice mapping based on the Auto-OSDF method in the entire Hunan Province were 92.47% and 0.87, respectively. The results obtained by the Auto-OSDF method show an average R^2 value of 0.926 compared to municipal-level statistical planting areas. These results indicate the effectiveness of the method in large-scale rice mapping in cloudy and rainy areas.

3) Under cloud contamination interference conditions, the decision-level fusion of optical and SAR features can more effectively mitigate the impact of cloud contamination on the accuracy of rice mapping compared to the feature-level fusion.

Acknowledgment

Thanks to ESA and CRASAC for the free data.

References

[1] R.G. Ni, J.Y. Tian, X.J. Li, D.M. Yin, J.W. Li, H.L. Gong, *et al.*, "An enhanced pixel-based phenological feature for accurate paddy rice mapping with Sentinel-2 imagery in Google Earth Engine," *ISPRS J. Photogramm. Remote Sens.*, vol. 178, pp. 282-296, 2021.

[2] Z. Yu, L. Di , S. Shrestha, C. Zhang , L. Guo, F. Qamar, et al., "RiceMapEngine: A Google Earth Engine-Based Web Application for Fast Paddy Rice Mapping," in IEEE Journal of Selected Topics in Applied Earth Observations and Remote Sensing, vol. 16, pp. 7264-7275, 2023, doi: 10.1109/JSTARS.2023.3290677.

[3] H.J. Yang, B. Pan, W.F. Wu, J.H. Tai, "Field-based rice classification in Wuhua county through integration of multi-temporal Sentinel-1A and Landsat-8 OLI data," *Int. J. Appl. Earth Observ. Geoinf.*, vol. 69, pp. 226-236, 2018.

[4] J.M. Salmon, M.A. Friedl, S. Frolking, D. Wisser, E.M. Douglas, "Global rain-fed, irrigated, and paddy croplands: A new high resolution map derived from remote sensing, crop inventories and climate data," *Int. J. Appl. Earth Observ. Geoinf.*, vol. 38, pp. 321-334, 2015.

[5] H.Q. Xu, Z. Tian, X.G. He, J. Wang, L.X. Sun, G. Fischer, et al., "Future increases in irrigation water requirement challenge the water-food nexus in the northeast farming region of China," *Agric. Water Manage.*, vol. 213, pp. 594-604, 2019.

[6] J. Elliott, D. Deryng, C. Mueller, K. Frieler, M. Konzmann, D. Gerten, *et al.*, "Constraints and potentials of future irrigation water availability on agricultural production under climate change," *Proc. Natl. Acad. Sci.* USA, vol. 111, pp. 3239-3244, 2014.

[7] J. W. Dong, X. M. Xiao, M. A. Menarguez, G. L. Zhang, Y. W. Qin, D. Thau, C. Biradar, *et al.*, "Mapping paddy rice planting area in northeastern Asia with Landsat 8 images, phenology-based algorithm and Google Earth Engine," *Remote Sens. Environ.*, vol. 185, pp. 142-154, 2016.

[8] M. Weiss, F. Jacob, G. Duveiller, "Remote sensing for agricultural applications: A meta-review," *Remote Sens. Environ.*, vol. 236, 2020, Art. no. 111402.

[9] Y.C. Zhang, W.B. Rossow, A.A. Lacis, V. Oinas, and M.I. Mishchenko, "Calculation of radiative fluxes from the surface to top of atmosphere based on ISCCP and other global data sets: Refinements of the radiative transfer model and the input data," *J. Geophys. Res. Atmos.*, vol. 109, 2004, Art. no. D19105.

[10] P.L. Wei, D.F. Chai, T. Lin, C. Tang, M.Q. Du, J.F. Huang, "Large-scale rice mapping under different years based on timeseries Sentinel-1 images using deep semantic segmentation model," *ISPRS J. Photogramm. Remote Sens.*, vol. 174, pp. 198-214, 2021.

[11] L.D. Robertson, A. Davidson, H. McNairn, M. Hosseini, S. Mitchell, D. de Abelleyra, *et al.*, "Using Dense Time-Series of C-Band Sar Imagery for Classification of Diverse, Worldwide Agricultural Systems," in *Proc. IEEE Int. Geosci. Remote Sens. Symp. (IGARSS)*, Yokohama, JAPAN, pp. 6231-6234, 2019.

[12] L. Liu, X.M. Xiao, Y.W. Qin, J. Wang, X.L. Xu, Y.M. Hu, *et al.*, "Mapping cropping intensity in China using time series Landsat and

Sentinel-2 images and Google Earth Engine," *Remote Sens. Environ.*, vol. 239, 2020, Art. no. 111624.
[13] Z. He, S. Li; M. Chang, Y. Liu, K. Liu, L. Wan, Y. Wang, et al., "Novel Harmonic-Based Scheme for Mapping Rice-Crop Intensity at a Large Scale Using Time-Series Sentinel-1 and ERA5-Land Datasets," in IEEE Transactions on Geoscience and Remote Sensing, vol. 62, pp. 1-23, 2024, Art no. 4406523, doi: 10.1109/TGRS.2024.3387559.
[14] P. Zhan, W.Q. Zhu, and N. Li, "An automated rice mapping method based on flooding signals in synthetic aperture radar time series," *Remote Sens. Environ.*, vol. 252, 2021, Art. no. 112112.
[15] S. Xu, X.L. Zhu, J. Chen, X.L. Zhu, M.J. Duan, B.W. Qiu, et al., "A robust index to extract paddy fields in cloudy regions from SAR time series," *Remote Sens. Environ.*, vol. 285, 2023, Art. no. 113374.
[16] X.Q. Jiang, S.J. Luo, S. Gao, S.H. Fang, Y.Y. Wang, K.L. Yang, *et al.*, "An automatic rice mapping method based on constrained feature matching exploiting Sentinel-1 data for arbitrary length time series," *Int. J. Appl. Earth Observ. Geoinf.*, vol. 114, 2022, Art. no. 103032.
[17] F. Wei, "Research on key technologies of cloud detection and restoration for optical remote sensing images," Ph.D. dissertation, School of Remote Sensing and Information Engineering, Wuhan University, Wuhan, Hubei Province, 2020.
[18]D. Xiang, X. Pan, H. Ding, J. Cheng and X. Sun, "Two-Stage Registration of SAR Images With Large Distortion Based on Superpixel Segmentation," in IEEE Transactions on Geoscience and Remote Sensing, vol. 62, pp. 1-15, 2024, Art no. 5211115.
[19]X. Zhao, Y. Wu, X. Hu, Z. Li and M. Li, "A Novel Dual-Branch Global and Local Feature Extraction Network for SAR and Optical Image Registration," in IEEE Journal of Selected Topics in Applied Earth Observations and Remote Sensing, vol. 17, pp. 17637-17650, 2024.
[20]D. Xiang, H. Ding, X. Sun, J. Cheng, C. Hu and Y. Su, "PolSAR Image Registration Combining Siamese Multiscale Attention Network and Joint Filter," in IEEE Transactions on Geoscience and Remote Sensing, vol. 62, pp. 1-14, 2024, Art no. 5208414.
[21]Q. Yu, Y. Jiang, W. Zhao and T. Sun, "High-Precision Pixelwise SAR–Optical Image Registration via Flow Fusion Estimation Based on an Attention Mechanism," in IEEE Journal of Selected Topics in Applied Earth Observations and Remote Sensing, vol. 15, pp. 3958-3971, 2022.
[22] H.S. Zhang and R. Xu, "Exploring the optimal integration levels between SAR and optical data for better urban land cover mapping in the Pearl River Delta," *Int. J. Appl. Earth Observ. Geoinf.*, vol. 64, pp. 87-95, 2018.
[23] M.I. Sameen, F.H. Nahhas, F.H. Buraihi, B. Pradhan, A.R.B.M. Shariff, "A refined classification approach by integrating Landsat Operational Land Imager (OLI) and RADARSAT-2 imagery for land-use and land-cover mapping in a tropical area," *Int. J. Remote Sens.*, vol. 37, pp. 2358-2375, 2016.
[24] D. Luo, H.X. Luo, G.P. Liu, X. Lei, and H.M. Feng, "Research on classification and fusion scale of sentinel-1A and sentinel-2A with different cloud cover," *Hubei Agric. Sci.*, vol. 59, no. 5, pp. 28-36, 43, 2020.
[25] M.J. Steinhausen, P.D. Wagner, B. Narasimhan, B. Waske, "Combining Sentinel-1 and Sentinel-2 data for improved land use and land cover mapping of monsoon regions," *Int. J. Appl. Earth Observ. Geoinf.*, vol. 73, pp. 595-604, 2018.
[26] J. Adrian, V. Sagan, and M. Maimaitijiang, "Sentinel SAR-optical fusion for crop type mapping using deep learning and Google Earth Engine," *ISPRS J. Photogramm. Remote Sens.*, vol. 175, pp. 215-235, 2021.
[27] Y. He, J. Dong, X. Liao, L. Sun, and P. Fu, "Examining rice distribution and cropping intensity in a mixed single- and double-cropping region in South China using all available Sentinel 1/2 images," *Int. J. Appl. Earth Observ. Geoinf.*, vol. 101, 2021, Art. no. 102351.
[28] B. Waske, S. van der Linden, "Classifying multilevel imagery from SAR and optical sensors by decision fusion," *IEEE Trans. Geosci. Remote Sens.*, vol. 46, pp. 1457-1466, 2008.
[29] X.Q., Jiang, H.Q., Du, S., Gao, S.H., Fang, Y., Gong, N., Han, Wang, , *et al.*, "An automatic rice mapping method based on an integrated time-series gradient boosting tree using GF-6 and sentinel-2 images," GIScience & Remote Sensing, vol.61,2024, Art. no. 2367807.
[30] A. ZUPANC, 2017. "Improving Cloud Detection with Machine Learning," https://medium. com/sentinel-hub/improving-cloud-detection-with-machine-learning-c09dc5d7cf13. 原 31
[31] S. Skakun, J. Wevers, C. Brockmann, G. Doxani, M. Aleksandrov, M. Batic, et al., "Cloud Mask Intercomparison eXercise (CMIX): An evaluation of cloud masking algorithms for Landsat 8 and Sentinel-2," *Remote Sens. Environ.*, vol. 274, 2022, Art. no. 112990. 原 35
[32] X.Q. Jiang, S.H. Fang, X. Huang, Y.H. Liu, and L.L. Guo, "Rice Mapping and Growth Monitoring Based on Time Series GF-6 Images and Red-Edge Bands," *Remote Sens.*, vol. 13, no. 4, 2021, Art. no. 579.
[33] Y. Guo and H. Ren, "Remote sensing monitoring of maize and paddy rice planting area using GF-6 WFV red edge features," *Comput. Electron. Agriculture*, vol. 207, 2023, Art. no. 107714.

Xueqin Jiang received the Ph.D. degree from the school of Remote Sensing Information Engineering, Wuhan University,Wuhan, in 2022. She is currently a lecturer with the School of Environment and Resources Science, Zhejiang A & F University.

Her research interests include remote sensing image processing, image interpretation and machine learning algorithms.

Song Gao received the master's degree from the School of Civil Engineering, Shandong University, Jinan, China, in 2018. He is currently pursuing the Ph.D. degree in College of Civil Engineering, Hunan University, Changsha, China.

His research interests include machine learning, intelligent design, and remote sensing image processing.

Huaqiang Du received the Ph.D. degree from Beijing Forestry University, Beijing, China, in 2005. He is currently a Professor with the School of Environment and Resources Science, Zhejiang A & F University, Hangzhou, China.

His research interests include forest carbon estimation with remote sensing techniques and forest resource monitoring using multisource remotely sensed data and digital image processing.

Shenghui Fang received the Ph.D. degree from Wuhan University, Wuhan, China, in 2009.
He is currently the Dean of the School of Remote Sensing and Information Engineering, Wuhan University.

He has authored more than 50 peerreviewed articles in international scientific journals. His research interests include remote

sensing, geographical information science, agricultural science, and big data mining.

Yan Gong received the Ph.D. degrees in photogrammetry and remote sensing from WHU, Wuhan, China, in 2007. He is currently a Professor of photogrammetry and remote sensing with the School of Remote Sensing and Information Engineering, WHU.

His research interests include hyperspectral remote sensing on agriculture, the phenotype analysis of hybrid rice, radiometric calibration of satellite and UAV images and the atmosphere correction of remote sensing images.

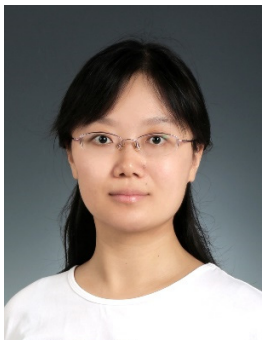

Ning Han received the Ph.D. degree from Zhejiang University, Zhejiang, China, in 2011. She is currently an Associate Professor with the School of Environment and Resources Science, Zhejiang A & F University, Hangzhou, China.

Her research interests include remote sensing monitoring of forest resources and estimation of carbon storage.

Yirong Wang received the B.S. degree in landscape architecture from Yangzhou University Guangling College, Yangzhou, China, in 2023,where she is currentlypursuing the M.S. degree.

Her research interests include land use and land cover change and carbon storage estimation using remotely sensed data.